

Demonstration Of A Continuously Guided Atomic Interferometer Using A Single-Zone Optical Excitation

M.S. Shahriar^{1,2}, Y. Tan², M. Jheeta², J. Morzinski², P.R. Hemmer², and P. Pradhan^{1,2}

¹*Department of Electrical and Computer Engineering, Northwestern University, Evanston, IL 60208*

²*Research Laboratory of Electronics, Massachusetts Institute of Technology, Cambridge, MA 02139*

We demonstrate an atomic interferometer in which the atom passes through a *single-zone* optical beam, consisting of a pair of bichromatic counter-propagating fields. During the passage, the atomic wave packets in two distinct internal states trace out split trajectories, guided by the optical beams, with the amplitude and spread of each wave-packet varying continuously, producing fringes that can reach a visibility close to unity. We show that the rotation sensitivity of this continuous interferometer (CI) can be comparable to that of the Borde-Chu Interferometer (BCI). The relative simplicity of the CI makes it a potentially better candidate for practical applications.

39.20.+q, 03.75.Dg, 04.80.-y, 32.80.Pj

Introduction : In a typical atomic interferometer[1-8], an atomic wavepacket is first split up by an atomic beam-splitter [9-13], then the two components are redirected towards each other by atomic mirrors. Finally, the converging components are made to interfere by another atomic beamsplitter. Here, we demonstrate an atomic interferometer where the atomic beam is split and recombined in a continuous manner. Specifically, in this interferometer, the atom passes through a single-zone optical beam, consisting of a pair of bichromatic counter-propagating fields that cause optically off-resonant Raman excitations. During the passage, the atomic wave packets in two distinct internal states couple to each other continuously, and the states each traces out a complicated trajectory, guided by the optical beams, with varying amplitudes and spreads of each wave-packet. Yet, at the end of the single-zone excitation, the interference fringe amplitudes can reach a visibility close to unity. One can consider this experiment as a limiting version of the so-called $\pi/2-\pi-\pi/2$ Raman atomic interferometer, proposed originally by Borde [1], and demonstrated by Kasevich and Chu *et al.* [2]. This configuration is potentially simpler than the Borde-Chu interferometer (BCI), eliminating the need for precise alignment of the multiple zones. Under circumstances of potentially practical interest, the CI may be able to achieve a rotational sensitivity comparable to that of the BCI, as described later. As such, the relative simplicity of the CI may make it an attractive candidate for measuring rotation and for other applications.

BCI and CI : In order to illustrate the CI, it is instructive to recall the BCI briefly, where the atom is assumed to be a three level system in the lambda configuration, with two low-lying levels $|a\rangle$ and $|b\rangle$, each of which is coupled to the level $|e\rangle$. The atom moves in the x direction through two counter propagating laser beams in the z direction, which are split in three equidistant zones, as illustrated in Fig. 1 (top). One of the laser beams couples $|a\rangle$ to $|e\rangle$, while the other couples $|b\rangle$ to $|e\rangle$. The $\pi/2$ Raman pulse in the first zone splits the atom into

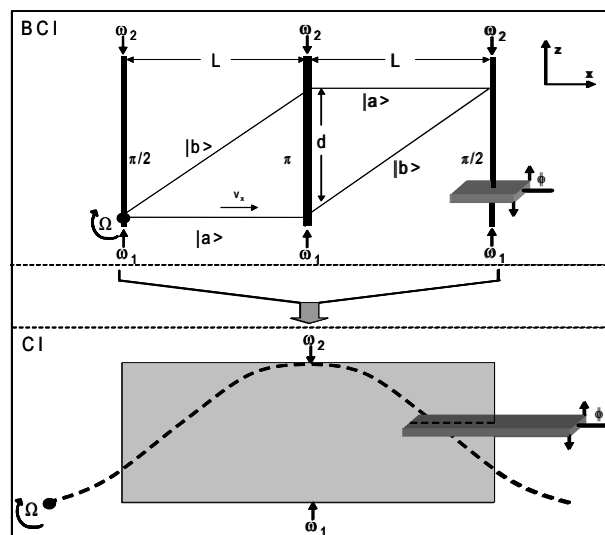


FIG. 1. Schematic illustration of the BCI as compared to the CI. In the BCI, the atom passes through three laser pulses of $\pi/2 - \pi - \pi/2$ arrangement. In the case of CI, the atom passes through one laser pulse of Gaussian shape. In each case, an external phase ϕ is applied by a glass plate that rotates along the x axis and the interferometer rotates around the z axis with an angular velocity Ω .

two components: the $|a\rangle$ part travels straight, while the $|b\rangle$ part picks up a transverse momentum of $2\hbar k$, where k is the average wavenumber of the two laser beams.

The π Raman pulse in the second zone redirects these trajectories, followed by a $\pi/2$ Raman pulse in the last zone, which returns the atom to a state where the fraction of the atoms in the $|a\rangle$ state, for example, depends on the phase shift ϕ applied to this zone, using a glass plate that rotates around the x axis. A signal corresponding to the population of level $|b\rangle$ thus varies sinusoidally with ϕ , with the fringe minimum occurring at $\phi=0 \pmod{2\pi}$. If the whole apparatus rotates at a rate Ω around the y axis, then the fringe minimum shifts by an amount given by $\delta\phi = 2\Omega A m/\hbar$, where A is the area enclosed by the trajectory of the split components of the wave packet and

m is the mass of the atom.

In contrast, the CI employs only a single zone, for which the profile in the \mathbf{x} direction (Gaussian, for example) is chosen to correspond to a 2π Raman pulse. The phase shift, ϕ , is applied to a part of this beam, as illustrated in Fig. 1 (bottom). For $\phi=0$, it is obvious that the atom will be in state $|a\rangle$ at the end of the interaction, just as in the case of the BCI. However, it may not be obvious how one would define an effective area for this interferometer, how the population in state $|b\rangle$, for example, would depend on the phase ϕ , and what would be the rotational sensitivity.

Numerical simulation : We show theoretically that in fact the functional behavior of the CI is very similar to that of the BCI. Here, we report briefly the key features of this analysis. A more detailed analysis is presented in reference [14]. Specifically, we show the calculated trajectories of the split components, then determine the rotational sensitivity, and use it to determine the effective area of the CI, defined as $A_{eff} = \hbar\delta\phi/2\Omega m$. Finally, we present our experimental results demonstrating the operation of the CI, manifested as interference fringes observed as a function of the phase ϕ . The formalism used in this analysis uses a quantized center-of-mass (COM) position for the atom along the z direction. In the electric dipole approximation, the Hamiltonian for the system can be written as:

$$H = \mathbf{P}_z^2/2m + H_0 + q\mathbf{r} \cdot (\mathbf{E}_1 + \mathbf{E}_2), \quad (1)$$

where \mathbf{E}_1 and \mathbf{E}_2 are the classical electric field vectors of the two counter-propagating lasers, \mathbf{P}_z is the COM momentum in the \mathbf{z} direction, H_0 is the internal energy, \mathbf{r} is the position of the electron with respect to the nucleus, and q is the electronic charge. We use as the basis the eigenstates of the non-interacting Hamiltonian, $|P_z\rangle \otimes |i\rangle \equiv |p, i\rangle$. Define ω_i as the energy of the i th ($i = a, b, e$) state, k_j , ω_j and ϕ_j as the wavenumber, the angular frequency and the phase, respectively, of \mathbf{E}_j , and Ω_j and δ_j as the Rabi frequency and the detuning, respectively, for the transition excited by \mathbf{E}_j ($j = 1, 2$). Considering counter-propagating laser fields $k_1 = -k_2 = k$, it can be shown [14] that this Hamiltonian creates transitions only between the following manifold of states for a fixed momentum p : $|p, a\rangle \leftrightarrow |p + \hbar k, e\rangle \leftrightarrow |p + 2\hbar k, b\rangle$. Let the amplitude of these three states be $\tilde{\alpha}$, $\tilde{\beta}$, and $\tilde{\xi}$ [15-19] within the manifold of a fixed momentum p . Since the laser beams are far detuned from resonance, we make the adiabatic approximation, which assumes that the intermediate state occupation is negligible and that we can set $\dot{\tilde{\xi}} \approx 0$. We then get the dynamics of an effective two level system $\psi_{eff} \equiv \begin{bmatrix} \tilde{\alpha}(p, t) \\ \tilde{\beta}(p + 2\hbar k, t) \end{bmatrix}$ by solving $i\hbar\dot{\psi}_{eff} = H_{eff}\psi_{eff}$, where the effective Hamiltonian is:

$$\tilde{H}_{eff}(p) = \hbar \begin{bmatrix} \frac{\Delta}{2} + \frac{\Omega_a}{2} & \frac{\Omega_a}{2} \\ \frac{\Omega_a}{2} & -\frac{\Delta}{2} + \frac{\Omega_a}{2} \end{bmatrix}. \quad (2)$$

with the effective Rabi frequency $\Omega_0 \equiv \Omega_1\Omega_2/(\delta_1 + \delta_2)$ and $\Delta \equiv (\delta_1 - \delta_2)/2$.

Ignoring any global phase factor which does not depend on p , we can get the expression for the system wavefunction at a time t for all p :

$$|\Psi(t)\rangle = \int dp \exp((p^2 + (p + 2\hbar k)^2)t/4m\hbar) (\tilde{\alpha}(p, t) |p, a\rangle + \tilde{\beta}(p + 2\hbar k, t) |p + 2\hbar k, b\rangle). \quad (3)$$

In our analysis of the rotational sensitivity, we apply this solution for the state vector for the case of a laser field with a Gaussian profile in the x direction. The position representation of the wavefunctions for the $|a\rangle$ and $|b\rangle$ states are then:

$$\psi_a(x, t) = \int dp \tilde{\alpha}(p, t) \exp\left(\frac{-ipx}{\hbar}\right), \quad (4a)$$

$$\psi_b(x, t) = \int dp \tilde{\beta}(p + 2\hbar k, t) \exp\left(\frac{-ipx}{\hbar}\right), \quad (4b)$$

and the probabilities for the atom to be in either state are:

$$P(a) = \int dp |\tilde{\alpha}(p, t)|^2, \quad (5a)$$

$$P(b) = \int dp |\tilde{\beta}(p, t)|^2. \quad (5b)$$

In order to do a phase scan in this system, we apply a phase-shift to the laser pulse starting from some position δl measured from the center of the pulse and extending in the direction of propagation of the atom. Such a scan can be realized by placing a glass plate in the path of the beam, inserted only partially into the transverse profile of the laser beams, and rotating it in the vertical direction. We perform our simulation on a Gaussian field discretized along the x direction, with the system rotating with an angular velocity Ω during the interaction time T . The phase shift for this interferometer is linear for infinitesimal rotations. Thus, an effective area for this interferometer can be defined as above. We choose to simulate a system with the following parameters: $\Omega_0 = 2\pi (7 \times 10^4)$ and $l = 3 \times 10^{-3}$ m, such that $\Omega_0 T = 3.3$. The atom is a Gaussian wavepacket with a $1/e$ spread of $1/k$, where $k = 8.0556 \times 10^6 \text{m}^{-1}$, corresponding to the wavelength of the laser, 780 nm. The wavepacket centroid trajectories in the CI are shown in Fig 2.[A] for $\phi = 0$. Here, the trajectories may appear to be completely separated from one another, however, note that the atomic wavepackets are highly overlapped, given the width of the wavepacket. The trajectories are plotted in Fig. 2[A] with no rotation in the system. If the system is rotating, there will be slight deviations in the trajectories, which lead to the rotational fringe shifts. Simulations are performed to determine the effective area

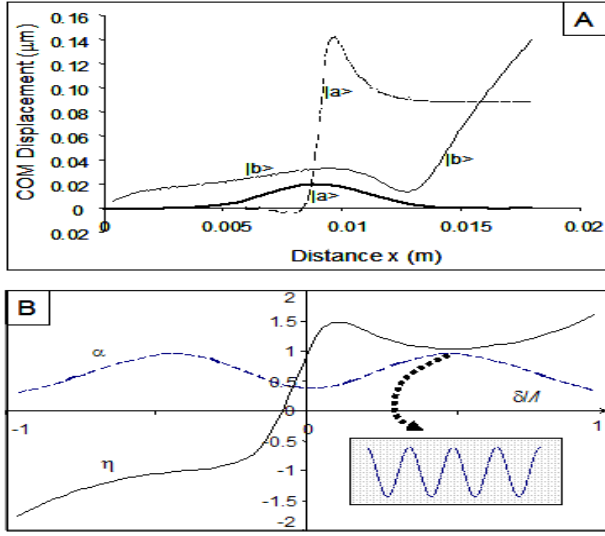


FIG. 2. [A] The trajectory of the split components in the CI, generated from numerical simulation. [B] The fringe amplitude (α) and the normalized effective area ($\eta \equiv A_{eff}/A_0$) vs. $\delta l/l$ for the CI from the same numerical simulation. (Inset) Simulated fringe amplitude vs. external phase ϕ at $\eta = .955$.

of the interferometer, as a function of the location of the the point of application of the phase shift.

In order to compare this rotation sensitivity with that of a BCI, we now need to know the area of a BCI that would correspond to the parameters of our system, the CI. To make this correspondence, note that most of the interaction in the Gaussian laser profile occurs within one standard deviation of the peak of the profile. Thus, it is reasonable to define an equivalent BCI with a zone-separation length of $L = 3 \times 10^{-3}$ m (so that the three-zone length is $2L$), which is the $1/e$ length of the Gaussian profile. The area of a BCI is given by $A_0 = L^2 2\hbar k / (mv_x)$. For $L = 3 \times 10^{-3}$ m, we get $A_0 = 2.7 \times 10^{-10}$ m².

With this value of A_0 we calculate [14] the variation of the fringe amplitude α and the normalized area ($\eta \equiv A_{eff}/A_0$) as a function of $\delta l/l$. These are plotted in Fig. 2 [B]. The maximum fringe contrast for our system is 0.955 and occurs at $\delta l/l = \pm 0.48$. The phase scan displaying this result is shown in the inset. The quality factor is approximately one for $|\delta l/l| > 0.25$, which means that if the phase is applied starting in this range of values, *our CI interferometer will provide the same rotation sensitivity as a BCI of the same size does* [14].

CI Experiment : Our experimental setup is shown schematically in Fig. 3[A]. A thermal ⁸⁵Rb atomic beam is collimated by two apertures, each of radius 50 μ m and separated by 112 mm. The interaction region is magnetically shielded by μ metal, with a magnetic bias field along the direction of the Raman beams, provided by Helmholtz coils.

The Ti-sapphire laser used in the experiment is locked to the $F=3 \rightarrow F'=3$ transition using a saturated absorp-

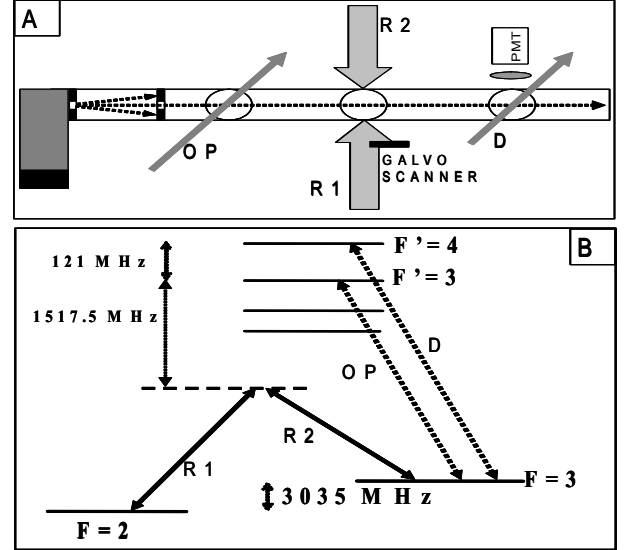


FIG. 3. [A] Schematic illustration of the experimental setup of our CI. Collimated thermal ⁸⁵Rb atoms are first optically pumped to prepare an initial state. Next, the atoms pass through an interaction zone containing a bias magnetic field and two Raman pulses (R_1 and R_2). A glass plate on a galvo scanner is inserted in the edge of R_1 . [B] Schematic illustration of the ⁸⁵Rb transitions employed in realizing the CI. Raman transition is realized between the ground states of $5^2S_{1/2}(F=3)$ and $5^2S_{1/2}(F=2)$ by two Raman beams R_1 and R_2 . To prepare an initial state, the $F=3$ ground state is optically pumped (OP) to the $F=2$ ground state via the state $5^2P_{3/2}(F'=3)$. The population of the $F=3$ state is detected (D) via a cycling transition to the $5^2P_{3/2}(F'=4)$ state, by a PMT.

tion cell. A beam at this frequency (OP in Fig.3[B]) is used to prepare the atom in the $F=2$ state via optical pumping. The detection beam (D in Fig. 3[B]) is generated by using an AOM at 120 MHz. To generate the Raman beams, another part of the laser is divided into two parts with a 50/50 beam splitter. One part (R_1) is upshifted through a 1.5 GHz AOM, and the other part (R_2) is downshifted through another 1.5 GHz AOM. The two 1.5 GHz AOMs are controlled by the same microwave generator, and so are phase-correlated with each other. The downshifted beam is red-detuned by 1.5 GHz from the $F=3$ to $F'=3$ transition, and the upshifted beam is red-detuned by 1.5 GHz from the $F=2$ to $F'=3$ transition. See Fig. 3[B] for a level diagram of the frequencies. Detection is performed by collecting the fluorescence using a photomultiplier tube (PMT). The bias field separates the magnetic sublevels ($F=2$ and $F=3$ have opposite sign g -factors) so that the Raman transition between $F=2$, $m_F=0$ and $F=3$, $m_F=0$ is shifted from the neighboring Raman transitions (e.g., $F=2$, $m_F=1$ and $F=3$, $m_F=1$) by nearly 1 MHz/Gauss. Given the transverse velocity spread which corresponds to a Raman linewidth of about 3.2 MHz FWHM (including transit time broadening), the use of a bias field of 2 Gauss enables us to resolve the sub-

level Raman transitions. The experiment is performed by exciting the $m_F=0$ to $m_F=0$ transition.

To scan the phase of the interference of the CI, we insert a 1mm thick glass plate mounted on a galvo scanner into an edge of a Raman beam. The galvo is mounted on a magnetic base and is driven by a BK Precision function generator. The beam that passes through the glass plate acquires a phase that varies with the angle of the plate. The intensity of the detected signal varies as the phase is scanned, and a plot of the observed population in state $F=3$ is shown in Figure 4[A]. To calibrate the phase scan produced by the glass plate, we perform a Mach-Zehnder optical interferometer experiment with the same scanner. Figure 4[B] shows the Mach-Zehnder interference pattern varying with the scanned phase. The data shown in Fig. 4 [A] is averaged over 512 traces, with a galvo scan rate of 32 Hz. The amplitude of the background (not shown) is about 5 times that of the fringe amplitude. This is mostly due to a combination of two factors: imperfection of the optical pumping in the first zone and residual optical pumping during the Raman interaction into $F=3$ state. No attempt is made to optimize the signal to noise ratio for this proof of principle experiment.

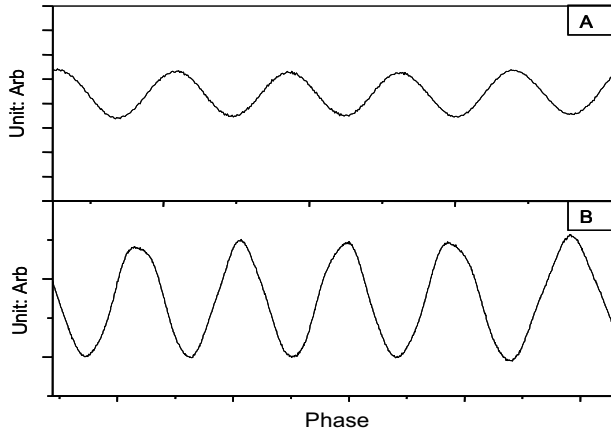


FIG. 4. [A] The observed atomic interference fringes in the CI, produced when a galvo scanner rotates a glass plate which produces a phase shift. [B] The corresponding optical fringes in a Mach-Zehnder interferometer using the same scanner. Here, one full fringe corresponds to an optical path length of $\lambda(=780\text{nm})$.

Discussion : The CI may be operationally simpler because it uses only one zone. In practice, this means that there is no need to ensure the precise parallelism of the three zones, as needed for the BCI. Therefore, the CI may be preferable to the BCI, given that the effective area and therefore the rotational sensitivity of the CI can be close to that of the BCI. One potential concern is that while the BCI can accommodate an effective length (separation between the first and the third zones: $2L$) as long as several meters, such a long interaction length for the CI would be impractical. On the other hand, an

interferometer that is several meters long is unsuited for practical usage such as inertial navigation. Therefore, it is likely that a practical version of the BCI would be much shorter (several cm's) in length and would reduce the rotational sensitivity drastically. This concern can potentially be overcome by using a slowed atomic beam (e.g., from a magneto-optic trap or Bose-condensate), so that the transverse spread of the split beams would be much larger, thereby compensating for the reduction in the longitudinal propagation distance. Under such a scenario, the CI would be simpler than the BCI, while yielding the same degree of rotational sensitivity.

This work was supported by DARPA grant No. F30602-01-2-0546 under the QUIST program, ARO grant No. DAAD19-001-0177 under the MURI program, and NRO grant No. NRO-000-00-C-0158.

-
- [1] C.J. Borde, Phys. Lett. A **140** (10), 1989.
 - [2] M. Kasevich and S. Chu, Phys. Rev. Lett. **67**, 181 (1991).
 - [3] L. Gustavson, P. Bouyer, and M. A. Kasevich, Phys. Rev. Lett. **78**, 2046 (1997).
 - [4] M. J. Snadden, *et al.*, Phys. Rev. Lett. **81**, 971 (1998).
 - [5] T.J. M. McGuirk, M. J. Snadden, and M. A. Kasevich, Phys. Rev. Lett. **85**, 4498 (2000).
 - [6] Y. Tan, J. Morzinski, A.V. Turukhin, P.S. Bhatia, and M.S. Shahriar, Opt. Comm. **206**, 141 (2002).
 - [7] D. Keith, C. Ekstrom, Q. Turchette, and D.E. Pritchard, Phys. Rev. Lett. **66**, 2693 (1991).
 - [8] D.S. Weiss, B.C. Young, and S. Chu, Phys. Rev. Lett. **70**, 2706 (1993).
 - [9] T. Pfau *et al.*, Phys. Rev. Lett. **71**, 3427 (1993).
 - [10] U. Janicke and M. Wilkens, Phys. Rev. A **50**, 3265 (1994).
 - [11] R. Grimm, J. Soding, and Yu.B. Ovchinnikov, Opt. Lett. **19**, 658 (1994).
 - [12] T. Pfau, C.S. Adams, and J. Mlynek, Europhys. Lett. **21**, 439 (1993).
 - [13] K. Johnson, A. Chu, T.W. Lynn, K. Berggren, M.S. Shahriar, and M.G. Prentiss, Opt. Lett. **20**, 1310 (1995).
 - [14] M.S. Shahriar, M. Jheeta, Y. Tan, P. Pradhan, and A. Gangat, quant-ph/0309147.
 - [15] P.M. Radmore and P.L. Knight, J. Phys. B. **15**, 3405 (1982).
 - [16] M. Prentiss, N. Bigelow, M.S. Shahriar and P. Hemmer, *Optics Letters*, **16**, 1695(1991).
 - [17] P.R. Hemmer, M.S. Shahriar, M. Prentiss, D. Katz, K. Berggren, J. Mervis, and N. Bigelow, Phys. Rev. Lett. **68**, 3148 (1992).
 - [18] M. S. Shahriar and P. Hemmer, *Phys. Rev. Lett.*, **65**, 1865(1990).
 - [19] M. S. Shahriar, P. Hemmer, D.P. Katz, A. Lee and M. Prentiss, *Phys. Rev. A*, **55**, 2272 (1997).